Journal of Chromatography A, 1410 (2015) 76–89

Contents lists available at ScienceDirect

Journal of Chromatography A

journal homepage: www.elsevier.com/locate/chroma

Possibilities of retention prediction in fast gradient liquid chromatography. Part 3: Short silica monolithic columns

Pavel Jandera*, Tomáš Hájek

Department of Analytical Chemistry, Faculty of Chemical, Technology, University of Pardubice, Studentská 573, 53210 Pardubice, Czech Republic

ARTICLE INFO

Article history:
Received 17 April 2015
Received in revised form 16 July 2015
Accepted 16 July 2015
Available online 20 July 2015

Keywords:
Gradient elution
Modeling of chromatography
Monolithic columns
Fast separations
Two-dimensional chromatography

ABSTRACT

We studied possibilities of prediction of the gradient elution data for alkylbenzenes, flavones and phenolic acids on two short octadecyl silica gel monolithic columns, namely a Chromolith Flash C18, 25 × 4.6 mm, and a "new generation" Chromolith High Resolution C18, 50 × 4.6 mm, in fast 1–2 min gradients. With fixed short gradient times and varying gradient ranges of acetonitrile concentration in water, high flow rates of the mobile phase (3–5 mL/min) could be used. The gradient elution data were predicted from four gradient models based on two-parameter and three-parameter isocratic retention equations. Various gradient retention models can be used for prediction of chromatograms and optimization of separation within a fixed gradient time. A two-parameter log–log model introduced in 1974 and a three-parameter model introduced in 1980 provided slightly more accurate prediction than the Linear Solvent Strength (LSS) semi-logarithmic two-parameter model, most frequently used in reversed-phase LC. A three-parameter model introduced in 1978 provided slightly improved accuracy of prediction of gradient data with respect to two-parameter models, in contrast to another, more recent three-parameter empirical model introduced in 2010 (which failed for gradients starting at a non-zero concentration of acetonitrile). Both a longer (5 cm) and more efficient Chromolith HR column and a shorter (2.5 cm) slightly less efficient Chromolith Flash column provide useful separations in fast gradients (1–2 min) at high flow rates (3.5–5 mL/min), especially in second dimension of two-dimensional LC × LC, in combination with HILIC separation on monolithic microcolumn in D1.

1. Introduction

Short analysis times become important in modern HPLC practice with the impact on the productivity of analytical laboratories. Fast generic gradient methods are important for drug discovery screening, raw material analysis, impurity profiling, pharmacokinetic studies and final product stability tests. Under gradient conditions, the numbers of peaks that can be separated within a fixed time significantly increase in comparison with isocratic elution. Gradient elution is a "must" to encompass potentially large differences between the sample components in 1–2 min, or even shorter separation times, in the second dimension of on-line two-dimensional LC × LC separations, where fast cycle frequency is imposed by a short time available for the separation of fractions transferred onto the second-dimension column [1].

Fast HPLC analysis can be accomplished on short very efficient UHPLC columns packed with sub-2 μm particles at a cost of very high operation pressures. Recently, we investigated the accuracy of prediction of gradient data in fast gradient chromatography (1–2 min) on short columns packed with fully porous [2] or superficially porous (core–shell) particles [3,4] with different chemistries of bonded stationary phases. We found that either 5 or 3 cm core–shell columns may provide comparable peak capacity in a fixed short gradient time with optimized gradient range.

In the present work, we extended the earlier investigation to two first and second generation silica-based monolithic C_{18} columns as another approach to fast separation at moderate pressures. Monolithic columns consist of a single-piece continuous separation media (rods) [5]. The structure of monolithic media can be represented as a network of small mesopores, which are responsible for the retention and separation selectivity, interconnected by large flow-through pores. This dual pore-size morphology provides good bed permeability and low flow resistance [6]. The first-generation silica-based monolithic columns allowed approximately three times faster analyses at the same operating pressure and comparable separation efficiency to the columns of the same length packed with 5 μm fully porous particles. Recently, new "second generation" Chromolith® HR columns with a tighter radial

* Corresponding author.
E-mail address: pavel.jandera@upce.cz (P. Jandera).

http://dx.doi.org/10.1016/j.chroma.2015.07.070
0021-9673/

pore distribution were introduced with claimed 50% higher efficiency and longer lifetime compared with the standard Chromolith columns [7,8]. Gritti et al. [9] investigated the gradient elution performance of 3.2 × 50 mm second generation silica monolithic columns, which showed peak capacities similar to the core–shell Kinetex columns.

Recently, we have applied the theory of gradient elution for prediction of retention data and optimization of fast second-dimension gradients in two-dimensional LC × LC [2,10–12]. Because of rapid changes in mobile phase composition during the fast gradients, short gradient times used in the repeated fraction transfer cycles impose that the column must be rapidly re-equilibrated to the initial conditions between the repetitive gradient analyses [13]. The re-equilibration can occur quickly, with less than three column volumes of conditioning solvent for flushing out the system dwell volume, V_D, and the column hold-up volume, V_M [14]. Recent investigation confirmed that gradient retention times are less sensitive to minor fluctuations in flow rate, temperature and mobile phase composition in comparison with isocratic data [15].

Gradient elution methods can be efficiently developed from an appropriate formal model, which however need not have any direct connection with the real retention mechanism, which may be rather complex. In the model equations, sample retention parameters are needed, which can be acquired in independent initial gradient or isocratic experiments. The most frequently used commercial optimization software, DryLab, employs two initial scouting gradients, a short one and a longer one, to find the optimum time of a simple (or segmented) gradient, yielding best resolution of a particular sample [16]. Running a few isocratic experiments with varying concentration of the strong solvent in the mobile phase is also suitable for the acquisition of the necessary input parameters to predict gradient behavior in a wide range of combinations of the adjustable experimental gradient parameters (flow rate, starting and final gradient concentrations, the volume of the mobile phase in the gradient, etc.). It is most important that the mobile phase composition range used for either isocratic or gradient parameter determination covers sufficiently broad range of not too low retention, with $k > 0.5$.

The equilibrium distribution between the stationary and the mobile phases is directly proportional to the retention factor, k, which is constant in isocratic chromatography, but continuously changes during gradient elution. If the instrumental gradient profile passes unchanged through the column (the gradient profile is not distorted) during the gradient run, the errors of predicted gradient data can be attributed to the errors in determination of the model parameters, irrespective of the elution mode (gradient or isocratic) used for their acquisition. However, there may be several non-thermodynamic sources of the deviations of the actual gradient profile, namely due to preferential adsorption on the column, rounding of the starting and of the final gradient parts, instrumental gradient delay function of the gradient mixer, etc., which may affected by the model parameters when the gradient mode is used for their acquisition, unlike to isocratic parameter acquisition. Fast steep gradients on short columns studied in this work are probably more liable to these errors than the longer ones.

The best way to find the answer is to compare the experimental retention data with the data predicted from a model, which is not affected by the particular kinetic effects of fast gradients. For this purpose, models with parameters acquired during gradient elution would not be as useful as the calculations with isocratic parameters, as the thermodynamics of retention is the same under both isocratic and gradient conditions. Hence deviations caused by non-thermodynamic sources in gradient elution should be clearly apparent from the discrepancies between the predicted and experimental gradient retention data.

In reversed-phase chromatography (RPLC), a simple semi-logarithmic (Linear Solvent Strength, LSS) isocratic model has been widely used to describe the effect of the volume fraction of the organic solvent, φ, on the retention factor, k, in aqueous-organic mobile phases [17]:

$$\log k = a - m \cdot \varphi \tag{1}$$

The parameters a (extrapolated log k in water) and m (the organic solvent strength parameter, sometimes denoted as S [16,18]) depend on the solute, stationary phase and type of the organic solvent.

Another simple log–log two-parameter Eq. (2) was originally introduced to describe the effects of the concentration of a more polar solvent in a less polar one, φ, on the retention factors, k in normal-phase separation systems with mixed organic mobile phases [17,19]:

$$\log k = a - m \cdot \log \varphi \tag{2}$$

k_0, a and m are experimental constants, k_0 being the retention factor in the pure strong solvent.

Various three-parameter model equations were employed to describe the effects of the mobile phase on retention [17,21–25]. These models have been reviewed and compared earlier elsewhere [25–28]. The most frequently used has been the second-order polynomial isocratic model published by Schoenmakers [20] (in fact, we published essentially the same model earlier, see [17]).

One of the first three-parameter models introduced a third parameter, b, into Eq. (2) to account for possible weaker retention of some samples in the less strong solvent [21]:

$$k = (b + a \cdot \varphi)^{-m} \tag{3}$$

Here, $1/(b)^m$ is the k in water ($\varphi = 0$). For very low b, Eq. (3) becomes identical with Eq. (2).

Recently, Neue and Kuss introduced an empirical model using three-parameters (k_{00}, b, a) [29]:

$$k = k_{00}(1 + a \cdot \varphi)^2 \cdot e^{-b \cdot \varphi/(1+a \cdot \varphi)} \tag{4}$$

k_{00} is k in pure water and a accounts for weaker retention in water. For very low a Eq. (4) becomes identical with Eq. (1). In this article, some parametrs of Eqs. (4), (9) and (15) were changed to avoid possible confusion with the terms traditionally used in the earlier literature: B was changed to b, c to φ, c_0,to A S to B, t_0 to t_m.

In the present work, we employ four isocratic models described by Eqs. (1)–(4) as the source of the model parameters for the calculations of gradient elution data for alkylbenzenes, phenolic acids and flavones in fast (1 min) gradients of acetonitrile in water starting at 0% and higher concentrations of acetonitrile, on short silica monolithic columns. Further, we investigate the effects of the gradient range on the peak capacity and we report new methods of the determination of the column efficiency in fast gradient elution. To our best knowledge, there has been no such systematic study of fast gradients on monolithic columns performed so far.

2. Theory

2.1. Prediction of gradient elution times (volumes) from the isocratic retention data

In linear gradient reversed-phase chromatography, the volume fraction of a polar organic solvent (acetonitrile, methanol) in water, φ, increases with the volume of the mobile phase that has flowed through the column in time t from the start of the gradient, $V = t F_m$:

$$\varphi = A + B \cdot V \tag{5}$$

Here, $B = (\varphi_G\text{-}A)/V_G$ is the gradient slope (ramp), independent of the flow rate of the mobile phase, F_m; $V_G = t_G.F_m$ is the gradient volume, i.e. the volume of the mobile phase from the start to the end of the gradient and t_G is the gradient time. $(\varphi_G\text{-}A)$ is the concentration range from the start, A, to the end of the gradient, φ_G.

For gradients with different ramps (B) and ranges (φ_G-A), the elution volumes, $V_{R(g)}$, can be predicted if the parameters of the gradient model are known. Both semi-logarithmic and log–log two-parameter models can be applied for direct prediction of retention times, $t_{R(g)}$, method development and optimization in gradient elution [30–33]. The model parameters should be determined in independent gradient or isocratic experiments. With the semi-logarithmic model parameters a, m, Eq. (1), the gradient elution time can be predicted using Eq. (6) [18,32–35]:

$$t_{R(g)} = \frac{1}{m \cdot B} \log\left[2.31mB \cdot \left(t_m \cdot 10^{a-m \cdot A} - t_D\right) + 1\right] + t_m + t_D \qquad (6)$$

The parameters a, m, of the log–log equation, Eq. (2) yield Eq. (7) for the gradient elution times [21,27,31]:

$$t_{R(g)} = \frac{1}{B}\left[(m+1)B\left(10^a \cdot t_m - t_D \cdot A^m\right) + A^{(m+1)}\right]^{\frac{1}{m+1}} - \frac{A}{B} + t_m + t_D \qquad (7)$$

t_m is the column hold-up time, $t_m = V_m/F_m$, A and B are the gradient parameters, Eq. (7), a and m are the best-fit regression constants of Eqs. (1) and (2).

V_D is the instrumental gradient dwell volume (which comprises the volume of the gradient mixer and of the connecting tubing between the mixer and the column inlet). At the start of the gradient, this volume is filled with the starting mobile phase, in which some less retained compounds may move for a shorter or a longer distance along the column before the front of the gradient. t_D is the corresponding gradient delay time. This effect may cause earlier than expected elution from the column and increases with decreasing dimensions of the column relatively to the instrumental dwell volume. Therefore, it is especially important to account for V_D when running fast gradients on short columns such as in the present work. Some weakly retained compounds may even completely pre-elute from the column in the dwell volume under isocratic conditions ($V_R < V_D$).

With some instruments, the dwell volume effect can be compensated by delayed injection with respect to the start of the gradient (at the cost of a longer analysis time). The prediction errors for samples strongly retained at the top of the column in gradients starting in pure water are often accounted for by simply adding the dwell volume to the predicted elution [35]. However, gradients starting at $A = 0$ may take long time. Starting gradients at a higher concentration of organic solvent usually significantly speeds up the separation. The partial pre-gradient migration of sample along the column becomes more significant and correction for the delay time, t_D, should be included in gradient models, such in Eqs. (6)–(9).

Increasing the number of parameters may improve the fit of the model to the experimental data; however a better fit may often be due to closer agreement to the data affected by experimental errors. Simpler models should be preferred in agreement with the Occam's razor scientific rule according to which the simplest of two or more competing theories should be preferred to the more complex, wherever possible.

Three-parameter or more complex retention model equations rarely provide direct analytical solution for $t_{R(g)}$ ($V_{R(g)}$) and usually are solved by less convenient numerical calculations. For the Schoenmakers second-order polynomial model, the analytical solution for gradient retention data has been obtained only after transformation to the Gaussian type of integral, resulting in a complicated equation including an error function (erf), which should be looked up in tables—this is not very practical. [20] The three-parameter Eq. (3), we derived in 1981 [21], provides closed form of only slightly more complex Eq. (8) for gradient elution times [36], the validity of which we have verified over years in various LC systems [37,38]:

$$t_{R(g)} = t_D + \frac{1}{a \cdot B}\left\{(m+1)a \cdot B\left[t_m - t_D(b + a \cdot A)^m\right] + (b + A \cdot a)^{m+1}\right\}^{1/(m+1)} - \frac{b + A \cdot a}{a \cdot B} + t_m \qquad (8)$$

The Neue–Kuss isocratic model equation, Eq. (4) [29], also provides analytical solution for gradient retention data, however more complex than our three-parameter gradient model described by Eq. (8). As this equation provides generally comparable (for gradients starting in water) or better results than Eq. (9), we prefer using the more simple Eq. (8).

$$t_R = \frac{1}{SB}\frac{(1+aA)^2 \ln\left(Bbk_{00}e^{-BA/(1+aA)}\left(t_m - \left(t_D/(1+aA)^2 k_{00}e^{-bA/(1+aA)} + 1\right)\right) + 1\right)}{1 - (a/b)(1+aA)\ln\left(Bbk_{00}e^{-BA/(1+aA)}\left(t_m - \left(t_D/(1+aA)^2 k_{00}e^{-bA/(1+aA)} + 1\right)\right) + 1\right)} + t_m + t_D \qquad (9)$$

where $t_R = V_R/F_m$ is the gradient retention time, $t_m = V_m/F_m$ is the column hold-up volume, $t_D = V_D/F_m$ is the gradient delay time and F_m is the flow rate of the mobile phase. Some symbols had to be changed to avoid confusion with generally used nomenclature, see the note to Eq. (4) on p. 5.

2.2. Gradient bandwidths

The sources of band broadening in fast gradient elution chromatography may include the contributions of the tubing placed upstream the column, the isocratic migration of the sample that takes place in the column dead volume, V_D, dispersion during band migration under gradient conditions to the column outlet, and dispersion in the tubing downstream the column to the detector [39].

The gradient bandwidths, w_g, are generally considerably narrower than the widths of the peaks eluted under isocratic conditions, due to continuously increasing elution strength of the mobile phase, which gradually decreases the solute local retention factor, k_i, at any actual position in the column and accelerates the migration velocity of the sample along the column during the gradient run, u_i:

$$u_i = \frac{u_0}{(1+k_i)} \qquad (10)$$

(u_0 is the flow velocity of the mobile phase). The dispersion by diffusion is directly proportional to the time the solute spends in the column, hence is inversely proportional to u_i, and gradually decreases as the solute moves from the top to the end of the column, unlike to sample migration under isocratic conditions (where k_i = const., u_i = const.) [16,31,33]. So-called gradient compression may cause some additional bandwidth decrease in gradient elution [16]. This effect originates in a slightly higher migration velocity along the column of the rear sample band end in the mobile phase with a higher elution strength with respect to the migration velocity of the front end in a weaker mobile phase. Obviously, this effect has minor importance on very narrow peak widths generated by short highly efficient columns as those used in the present work.

It is generally accepted that the gradient bandwidths w_g are principally controlled by the actual solute dispersion in the mobile phase at the time of elution ($\varphi = \varphi_e$) and can be—to first approximation—estimated as the bandwidths under isocratic conditions, with the local retention factor at the end of column at elution, $k_i = k_e$ [16,31,32,40,41] The bandwidths may be slightly affected by extra-column contributions. Whereas, the band broadening in the tubing between the sample injector and the column is subject to the same gradient compression as the injected sample volume, the peaks eluted from the column experience the dispersion in the tubing connecting the column to the detector. To correct for this effect, we estimated this extra-column band broadening by measuring the peak widths with the column disconnected from the chromatographic system:

$$w_{(g)cor} = \sqrt{w^2_{(g)\,exp} - w^2_{ec}} = \frac{4 \cdot t_m}{\sqrt{N}}\,(1 + k_e) \tag{11}$$

($w_{g,cor}$ is the gradient bandwidth in time units, corrected for the extra column contributions, $w_{g,ec}$, and k_e is the local retention factor at the end of the column at the time of the solute elution, which can be calculated for various retention models). N is the number of theoretical plates of the column, which—unlike to isocratic elution—cannot be calculated directly from the gradient retention times and bandwidths. Hence, N measured under isocratic conditions at the time of elution is usually employed in Eq. (11). Combining the appropriate model retention equation, such as Eqs. (1)–(4) with the corresponding equation for gradient elution time (Eqs. (6)–(9), as appropriate), we can calculate the retention factors at any time and position in the column, k_i, hence also k_e at the end of the column [4]. For example, the semi-logarithmic retention model yields Eq. (12), the log–log model Eq. (13) and the three-parameter model, based on Eqs. (3) or (4) result in Eqs. (14) and (15):

$$k_e = \frac{1}{2.31mB \cdot t_m + 10^{(mA-a)}} \tag{12}$$

$$k_e = k_0\left[(m+1)Bk_0 \cdot t_m + A^{(m+1)}\right]^{-m/(m+1)} \tag{13}$$

$$k_e = k_0\left[(m+1)B \cdot b\,[t_m] + (a + A \cdot b)^{(m+1)}\right]^{-m/(m+1)} \tag{14}$$

$$k_e = \frac{k_{00}e^{-b\cdot A/(1+a\cdot A)}}{B \cdot b \cdot k_{00}e^{-b\cdot A/(1+a\cdot A)} + 1} \cdot \left(\frac{1 + a \cdot A}{1 - (a/b)\,(1 + a \cdot A)\ln\left(B \cdot b \cdot k_{00}e^{-b\cdot A/(1+a\cdot A)}\right) + 1}\right)^2 \tag{15}$$

The experimental bandwidths may be slightly narrower than the w_g, calculated from Eq. (11), due to the "additional gradient bandwidth compression", which may occur as the trailing edge of the sample moves slightly faster in a mobile phase with higher elution strength than the leading edge in a weaker mobile phase [42]. Poppe et al. [43] introduced a correction factor for this effect, which was later studied in more detail [44,45]. However, the experimental studies indicate that the additional band compression usually has minor effect on very narrow peaks in fast gradient elution.

As the elution strength of the mobile phase and the sample mobility in the column increases during gradient elution, the time available for band dispersion by diffusion decreases from the upper to the lower end of the column, so that the peak widths at the time of elution are more narrow than they would be should they be eluted in the starting mobile phase. The column plate number, N, (and the height equivalent to a theoretical plate, H,) depend more or less on the composition of the mobile phase. N may slightly change during the gradient elution [41], depending to some extent on the gradient profile controlling the k_e of the individual sample compounds. Peak widths at the time of elution are approximately constant for all sample compounds in gradient elution [39], hence the average bandwidth, $\bar{w}_{(g)}$, can be used to estimate the gradient plate numbers, $N_{(g)}$, from Eq. (16), to first approximation:

$$N_{(g)} = 16\left[\frac{t_m\,(1 + k_e)}{\bar{w}_{(g)}}\right]^2 \tag{16}$$

3. Experimental

3.1. Materials

Acetonitrile, LiChrosolv grade, was purchased from Merck (Darmstadt, Germany). Water was purified using a SG Ultra Clear UV water purification system (SG, Hamburg, Germany). Ammonium acetate and formic acid (≥98%) were purchased from Sigma-Aldrich (St. Louis, MI, USA). Buffered mobile phases containing 10 mM ammonium acetate were prepared by dissolving the appropriate weighed mass of ammonium acetate in water and adjusting the pH to 3.1 by adding a few drops of formic acid. The mobile phases were filtered using a 0.45 μm filter (Millipore, Bedford, MA, USA) and degassed by ultrasonication.

Alkylbenzene standards (benzene to *n*-pentylbenzene), uracil, phenolic acids and flavonoid compounds were obtained from Sigma-Aldrich (St. Louis, MI, USA). The stock solutions of *n*-alkylbenzene standards (20 g/L) were prepared in 1:1 aqueous acetonitrile and the stock solutions phenolic acid and flavonoid standards (100 mg/L) prepared in 1:1 aqueous methanol. The working standard solutions were obtained by appropriate dilution with the mobile phase. The list of phenolic acids and flavone solutes is given in Table 1.

3.2. Columns

Two commercial silica-based monolithic octadecyl columns were tested (both from Merck, Darmstadt, Germany):

1. A Chromolith Flash RP-18e, 25 × 4.6 mm, i.d. first generation column, manufacturers' declared stationary phase properties: 18% C, pore volume 1 mL/g, endcapped, mesopore size 13 nm, macropore size 2 μm, surface area 300 m^2/g, total porosity >80%
2. A Chromolith HighResolution RP-18e 50 × 4.6 mm i.d. second generation column, manufacturers' declared stationary phase properties: total pore volume 2.9 mL/g, endcapped, mesopore size 15 nm, macropore size 1.15 μm, surface area 250 m^2/g. For first dimension of two-dimensional comprehensive LC × LC, a zwitterionic monolithic microcolumn BiGDMA-MEDSA, 210 × 0.53 mm, i.d. [46] was used in on-line combination with either monolithic column in the second dimension.

Table 2 lists the properties of the two monolithic columns used in this work, a shorter, l = 25 mm Chromolith Flash RP-18e, first generation column, and a longer, l = 50 mm Chromolith HighResolution RP-18e second generation column: the monolith-specific area, S, the average diameter of macropores MaP, and mesopores, MeP, the column hold-up volume, V_m, measured with uracil as an inert marker compound, the column porosity, ε_T, the number of theoretical plates at isocratic conditions, $N_{(iso)}$, the gradient plate number, $N_{(g)}$, calculated using Eq. (16), and the height equivalents

Table 1
Phenolic acid, flavone and alkybenzene standards.

No.	Phenolic acid	No.	Flavone	No.	Flavone
1	Gallic acid	13	(-)-Epicatechin	27	Myricetin
2	Protocatechuic acid	14	(+)-Catechin	28	Esculin
3	*p*-Hydroxybenzoic acid	15	Flavon	29	Esculetin
4	Salicylic acid	16	7-Hydroxyflavon	30	Scopoletin
5	Vanillic acid	17	Apigenin	31	4-hydroxycoumarin
6	Syringic acid	18	Lutheolin	32	7-hydroxycoumarin
7	4-Hydroxyphenylacetic acid	19	Quercetin		
8	Caffeic acid	20	Rutin	Acr.	Alkylbenzene
9	Sinapic acid	21	Naringin	B	Benzene
10	*p*-Coumaric acid	22	Biochanin A	MB	Methylbenzene
11	Ferulic acid	23	Naringenin	EB	Ethylbenzene
12	Chlorogenic acid	24	Hesperetin	PrB	Propylbenzene
		25	Hesperidin	BB	Butylbenzene
		26	Morin	PeB	Pentylbenzene

to theoretical plate, H, determined from the average bandwidths, $w_{(g)exp}$, corrected for the extra-column band broadening:

$$H = \frac{N_{(g)}}{l} = \frac{16\left[\frac{t_m(1+k_e)}{\sqrt{w^2_{(g)exp}-w^2_{ec}}}\right]^2}{l} \quad (17)$$

3.3. Equipment

A 1200 series Rapid Resolution LC liquid chromatograph (Agilent, Palo Alto, CA, USA) equipped with a binary pump, a degasser, an auto-sampler, a diode-array UV detector and a thermostated column compartment was used in all single-dimension experiments.

In the comprehensive 2D setup, an 1100 series Agilent liquid chromatograph (Agilent, Palo Alto, CA, USA) equipped with a microflow binary pump, a degasser, an autosampler, a diode-array UV detector and a thermostated column compartment was used in the first dimension. A 1200 series Agilent Rapid Resolution LC operated at 600 bar and 5 mL/min, close to the operation pressure and flow rate limits, was used for fast second-dimension gradient runs. The first-dimension and the second-dimension columns were connected via an electronically controlled high-pressure ten-port 2-position valve (Valco, Houston, TX, USA) equipped with two identical 10 μL sampling loops, as the fraction transfer interface. The outlet of the second-dimension column was connected to the diode-array photometric detector of the 1100 liquid chromatography, to facilitate the export of the detector data for further processing.

3.4. Methods

The isocratic retention data used for the determination of the parameters *a, m, k_{00}, b*, of Eqs. (1)–(4) were measured in premixed mobile phases at different concentrations of acetonitrile in water and the parameters of linear and nonlinear dependences were calculated with statistical software Adstat (TriloByte Statistical Software, Czech Republic). The separations were repeated twice. The concentration range of isocratic separations used for the acquisition of the best fit equation parameters was selected to yield $k > 0.3$; i.e. 30–70% acetonitrile for alkylbenzenes, 3–15% acetonitrile for phenolic acids and 10–30% acetonitrile for flavones on the Chromolith Flash RP-18e column and 30–80% acetonitrile for alkylbenzenes, 3–15% acetonitrile for phenolic acids and 15–35% acetonitrile for flavones on the Chromolith HighResolution RP-18e column. The flow rate under isocratic conditions was set at 3 mL/min.

The column hold-up volumes (Vm) were measured as the elution volumes of non-retained uracil (Table 2). The temperature was set to 40 °C in all experiments. Experimental gradient delay volume of the 1200 series Rapid Resolution chromatograph (VD = 0.944 mL) were measured by running a linear gradient of 0.1% acetone in pure acetonitrile [30,34,39]. The bandwidths evaluated by the chromatography data station at the half peak heights were re-calculated to the bandwidths at the baseline (4σ), wg,exp, and corrected for the extra-column contributions (Eq. (11)) (w_{ec} = 0.02 mL).

In gradient experiments, 1 μL of the alkylbenzenes and 5 μL of the samples containing phenolic acids and flavones were injected. The temperature was kept at 40 °C and the flow rate at 5 mL/min. The gradient time was set to 1 min for the separation of alkylbenzenes and to 2 min for the separation of phenolic acids and flavones. The peaks were identified on the basis of isocratic retention data, UV–vis spectra and coeluting compounds were detected in repeated experiments with standard addition. The differences in the elution volumes in repeated gradient experiments were in the range of 1–6 μL, which corresponds to 0.07 s or less.

In the two-dimensional comprehensive LC × LC experiments, the whole effluent from the first-dimension microcolumn was transferred in-line to the second-dimension column in subsequent fractions collected alternately in two loops (10 μL) of a 10-port switching valve interface between the first-dimension and the

Table 2
Properties of the columns tested: HETP, height equivalent to a theoretical plate; *N*,number of theoretical plates in a column under isocratic condition $N_{(iso)}$; *L*, column length; *I.D.*, inner diameter; V_M, hold-up volume (uracil); ε_T, total column porosity; *S*, specific surface area; $HETP_{(iso)}$ for butylbenzene in 50% ACN.

Column	$L \times I.D.$ (mm)	V_M (mL)	ε_T	macropore (μm)	mesopore (nm)	S (m^2/g)	$HETP_{(iso)}$ (μm)	$N_{(iso)}$
Chromolith® Flash RP-18e (1st generation) (Merck, Darmstadt, Germany)	25 × 4.6	0.383	0.922	2.00	13	300	8.3	3000
Chromolith® HighResolution RP-18e (2nd generation) (Merck, Darmstadt, Germany)	50 × 4.6	0.760	0.914	1.15	15	250	7.8	6300
zwitterionic polymethacrylate monolithic microcolumns – BiGDMA-MEDSA [43]	210 × 0.53	0.034	0.714	–	–	-	27.5	7000

Table 3
Average experimental delay volume, $V_{D,exp}$, (without column for flow rate 1–5 mL/min) and $V_{D,calc}$ delay volume, calculated from the experimental V_R of alkylbenzene (MB-PeB) for three retention models (Eqs. (6)–(8)) on Chromolith Flash and Chromolith HighResolution columns. Gradient: 0–100% ACN in 1 min; flow rate 5 mL/min.

column	$V_{D,calc}$ (mL)			$V_{D,exp}$ (mL)
	log k-φ	log k–og φ	k-φ	
Chromolith Flash	0.950 ± 0.041	0.943 ± 0.053	0.949 ± 0.037	0.944 ± 0.030
Chromolith HighResolution	0.959 ± 0.039	0.908 ± 0.019	0.912 ± 0.012	

second-dimension columns. The collecting loops were only partially filled and the exact volume of the collected fractions was set by the switching cycle time. The flow rate in the second dimension was set at 5 mL/min, the flow rate in the first dimension was set to 4 μL/min, and the switching valve cycle time was adjusted to match the desired fraction volume at the pre-set second-dimension gradient time 1 + 0.5 min column re-equilibration time, or 0.8 + 0.4 min). The first-dimension column temperature was set at 60 °C and the second-dimension temperature at 50 °C.

4. Results and discussion

4.1. Separation efficiency of Chromolith columns

Fig. 1 shows van Deemter graphs of the height equivalent to a theoretical plate, H, versus the linear flow velocity of the mobile phase, u, for alkylbenzenes on the two monolithic columns, in 60% acetonitrile/water as the mobile phase. The columns show optimum performance (minimum of the H–u plots) at u = 2.5 mm/min, i.e. at 2.2 mL/min The shorter 25 mm 1st generation Chromolith Flash RP-18e column shows H_{min} = 10 μm (at 5 mL/min the efficiency slightly decreases to H_{min} = 12 μm). For the longer 50 mm, 2nd generation Chromolith High Resolution RP-18e column H_{min} = 8 μm; and decreases to H = 10 μm. at 5 mL/min. (For the smallest molecule of benzene, the efficiency is slightly lower, approximately 11 μm at 5 mL/min, which may be possibly due to the differences in pore morphology between the two types of silica monoliths). The efficiency of the Chromolith High Resolution RP-18e column is comparable to a column packed with 3 μm particles.

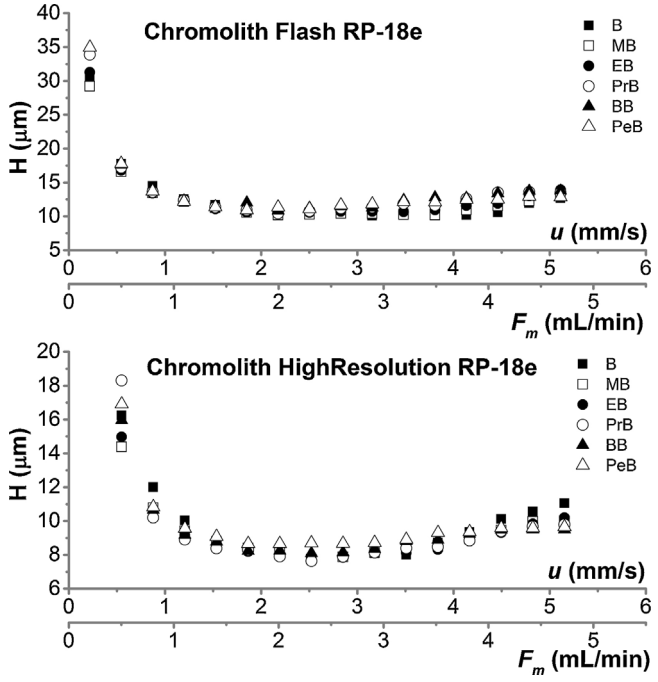

Fig. 1. Van Deemter plots for a Chromolith Flash and Chromolith HighResolution columns. HETP – height equivalent to a theoretical plate; u – linear mobile phase velocity; F_m – flow rate; mobile phase: 60% aqueous acetonitrile; temperature: 40 °C.

Both columns show only marginal loss of efficiency at increasing flow rate and can be easily used for fast gradients at 4–5 mL/min in two-dimensional HPLC.

4.2. Prediction of retention times in fast gradients on monolithic columns

4.2.1. Model Equation Parameters

In our recent study of fast gradients on core–shell columns, the gradient retention models described by Eqs. (6) and (7) yielded comparable accuracy of prediction of gradient elution volumes, (slightly better for the log k–log φ retention model than for the semi-logarithmic LSS (log k–φ) model Eq. (6). In the present work, we applied for direct prediction of elution times of alkylbenzenes, phenolic acids and flavones also the three-parameter model equations, Eqs. (8) and (9), in addition to the Eqs. (6) and (7). The parameters of the equations were determined in the isocratic scouting experiments using non-linear regression with ADSTAT software. Fig. S1 in the Supplementary internet material illustrates the agreement between the experimental data and the best-fit model isocratic retention factors of alkylbenzenes (from benzene, B, to pentylbenzene, PeB) on the Chromolith Flash (A–D) and Chromolith HighResolution (E–H) columns. The semi-logarithmic model (Eq. (1)) shows some negative deviations in the high retention range (Fig. S1 A, E). With the log–log model (Eq. (2)), only much weaker slight positive deviations are apparent in the weak retention range (Fig. S2 B, F). The three-parameter model equations, Eqs. (3) and (4), show equal agreement with the experimental data (Fig. S1, C–H); hence single plots are shown for both three-parameter models. The parameters a, m, k_{00}, b, evaluated from the isocratic sets of data and employed in the four gradient prediction models, Eqs. (6)–(9), are listed in the Supplementary internet material, Table S1 for alkylbenzenes and Table S2 for phenolic acids and flavones. The standard deviations (SD) of the parameters were determined to indicate potential gross errors in the mobile phase range used for the data acquisition.

The parameters m of Eq. (1) for phenolic acids on the Chromolith HR RP-18 in Table S2 are significantly higher for the acids in comparison with alkylbenzenes because of significantly greater decrease of retention at increasing acetonitrile concentration. The parameters a, m of the three-parameter Eq. (3) and their SDs of phenolic acids and flavones are comparable with lower alkylbenzenes, except for weakly retained gallic acid, sinapic acid, esculin, catechin and epicatechin, where the parameters are statistically unreliable. For most flavones, the additional parameter b is low, or even insignificant. The parameters k_{00},a, b of the three-parameter Eq. (4), for sinapic acid, epicatechin, catechin, esculin hydroxyflavone and rutin could not be reliably determined because of too low retention of these compounds, so that the gradient model Eq. (9) cannot be applied to these compounds.

4.2.2. Prediction of Gradient Times

Table 4 lists the experimental and predicted gradient retention times of alkylbenzenes in fast 1 min gradients from 0 to 100% and from 50 to 100% acetonitrile in water on the two Chromolith columns. All alkylbenzenes elute before the end of the gradient (1 + 0.19 min instrumental dwell time). The agreement between the experimental gradient elution times of alkylbenzenes and the

Table 4
Experimental, $t_{R,exp}$, and calculated, $t_{R,calc}$, model Eqs. (6–9) elution times for alkylbenzenes on the Chromolith Flash and Chromolith HighResolution column. Gradient: 0–100% ACN in 1 min and 50–100% ACN in 1 min; flow rate 5 mL/min. Δt_R = % differences between the calculated and the experimental t_R.

Gradient 0–100% acetonitrile in 1 min

		Chromolith Flash							
		log k–φ (Eq. 6)		log k–log φ (Eq. 7)		k–φ (Eq. 8)		k–φ (Eq. 9)	
Comp.	$t_{R,exp}$ (min)	$t_{R,calc}$ (min)	Δt_R (%)	$t_{R,calc}$ (min)	Δt_R (%)	$t_{R,calc}$ (min)	Δt_R (%)	$t_{R,calc}$ (min)	Δt_R (%)
B	0.68	0.65	4.71	0.71	3.37	0.68	0.41	0.68	0.12
MB	0.78	0.77	0.83	0.79	0.66	0.78	0.40	0.78	0.27
EB	0.85	0.86	0.98	0.85	0.46	0.86	0.72	0.85	0.64
PrB	0.92	0.93	1.37	0.92	0.71	0.92	0.81	0.92	0.79
BB	0.97	0.98	0.88	0.98	1.06	0.98	0.82	0.98	0.93
PeB	1.02	1.02	0.20	1.04	1.19	1.03	0.88	1.04	1.23
average	–	–	1.49	–	1.24	–	0.67	–	0.66
		Chromolith HighResolution							
		log k–φ (Eq. 6)		log k–log φ (Eq. 7)		k–φ (Eq. 8)		k–φ (Eq. 9)	
Comp.	$t_{R,exp}$ (min)	$t_{R,calc}$ (min)	Δt_R (%)	$t_{R,calc}$ (min)	Δt_R (%)	$t_{R,calc}$ (min)	Δt_R (%)	$t_{R,calc}$ (min)	Δt_R (%)
B	0.87	0.84	3.59	0.86	0.90	0.85	1.65	0.85	1.78
MB	0.95	0.94	0.83	0.94	1.18	0.94	0.89	0.94	1.00
EB	1.01	1.01	0.60	1.00	0.61	1.00	0.32	1.00	0.40
PrB	1.06	1.08	1.20	1.07	0.22	1.07	0.35	1.07	0.39
BB	1.11	1.13	0.98	1.12	0.81	1.12	0.80	1.13	1.11
PeB	1.16	1.16	0.37	1.18	1.28	1.17	0.68	1.18	1.93
average	–	–	1.26	–	0.84	–	0.78	–	1.10

Gradient 50–100% acetonitrile in 1 min

		Chromolith Flash							
		log k–φ (Eq. 6)		log k–log φ (Eq. 7)		k–φ (Eq. 8)		k–φ (Eq. 9)	
Comp.	$t_{R,exp}$ (min)	$t_{R,calc}$ (min)	Δt_R (%)	$t_{R,calc}$ (min)	Δt_R (%)	$t_{R,calc}$ (min)	Δt_R (%)	$t_{R,calc}$ (min)	Δt_R (%)
B [a]	0.17	–	–	–	–	–	–	–	–
MB	0.22	0.24	6.24	0.21	3.75	0.22	0.09	0.26	16.04
EB	0.30	0.33	9.85	0.30	0.37	0.31	2.74	0.28	6.24
PrB	0.41	0.44	8.47	0.41	0.19	0.42	2.00	0.33	19.87
BB	0.52	0.55	6.07	0.52	0.84	0.53	1.31	0.38	26.23
PeB	0.63	0.64	2.52	0.63	0.67	0.63	0.44	0.44	30.30
average	–	–	6.63	–	1.16	–	1.32	–	19.76
		Chromolith HighResolution							
		log k–φ (Eq. 6)		log k–log φ (Eq. 7)		k–φ (Eq. 8)		k–φ (Eq. 9)	
Comp.	$t_{R,exp}$ (min)	$t_{R,calc}$ (min)	Δt_R (%)	$t_{R,calc}$ (min)	Δt_R (%)	$t_{R,calc}$ (min)	Δt_R (%)	$t_{R,calc}$ (min)	Δt_R (%)
B	0.32	0.33	2.54	0.30	6.04	0.32	1.92	0.37	13.48
MB	0.41	0.43	5.07	0.40	4.29	0.41	1.48	0.39	4.88
EB	0.51	0.54	5.63	0.49	3.42	0.50	1.78	0.42	15.80
PrB	0.62	0.66	5.04	0.61	2.43	0.61	1.81	0.46	22.64
BB	0.73	0.76	3.31	0.72	1.88	0.72	1.91	0.52	26.95
PeB	0.84	0.85	1.03	0.83	1.59	0.83	1.29	0.57	29.90
average	–	–	3.77	–	3.27	–	1.70	–	18.94

[a] Elution before gradient in 50% ACN.

elution times predicted from the four gradient models characterized by Eqs. (6)–(9) for the 0–100% ACN gradients was satisfactory for all models with the gradients starting at 0% acetonitrile. The percent differences between the experimental and the predicted retention times were less than 1.4% for the model Eqs. (6)–(8) on the two Chromolith columns, except the prediction of the two-parameter models for benzene. There are some minor differences among the individual models. Whereas, the differences between the predicted and experimental retention times were within 0.04 min for the usually employed semi-logarithmic (LSS) model (Eq. (6), the log–log (Eq. (7)) and the simple three-parameter (Eq. (8)) models show the agreement within 0.02 min.

In the gradients starting at 50% acetonitrile, the elution times are considerably shorter than in the full-range gradients (0–100% acetonitrile). From the 25 mm Chromolith Flash column, the least retained solute, benzene, even pre-elutes in the gradient dwell time, before 1 min, under isocratic conditions (in 50% acetonitrile). The differences between the predicted and experimental elution times of alkylbenzenes in the 50–100% ACN gradients were 2.7% or less for the three-parameter model, Eqs. (8) and (4) 3% or less for the two-parameter log–log model, Eq. (7) but up to 10% for the two-parameter semi-logarithmic (LSS) model, Eq. (6). On the other hand, the recent three-parameter model, Eq. (9), shows very high deviations of predicted retention times (up to 30%) in gradients starting at 50% ACN. The model equation is much more complex than with the other models and, probably, there may be an error in the implementation of the starting gradient concentration, A, in the model in the original source [27].

Fig. 2 shows the separation of phenolic acids and flavonoids in a 2 min gradient 3–60% ACN on a Chromolith High Resolution column. The numbers of peaks are as in Table 1. The % differences, Δt between the experimental and predicted elution times in Table 5 are in approximate agreement with the results for alkylbenzenes in Table 4. Here, the log–log two-parameter model (Eq. (7)) showed

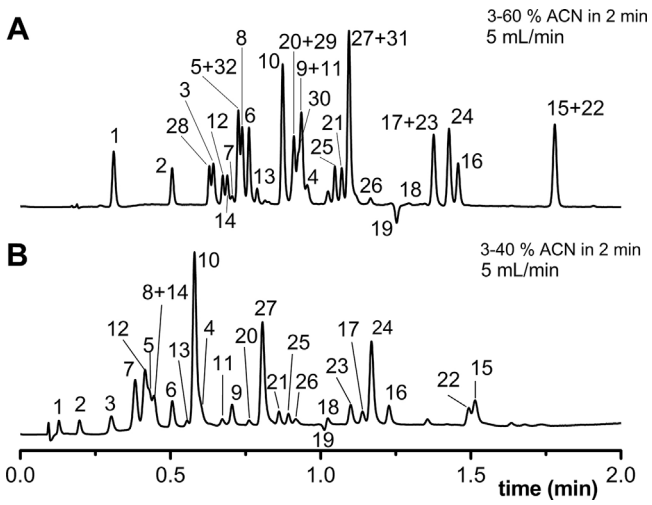

Fig. 2. Chromatograms of 32 phenolic and flavone compounds in 2-min gradients. (A) Chromolith HighResolution, 3%–60% acetonitrile; (B) Chromolith Flash, 3%–40% acetonitrile. Mobile phase: 0.05 mol/L aqueous ammoniumacetate + acetonitrile; flow rate: 5 mL/min; temperature: 40 °C. The numbers of peaks are as in Table 1.

the best results (3.2% mean deviation of the predicted retention times from the experiment), followed by the three-parameter model (Eqs. (8) and (4) 5% deviation) except for protocatechuic acid). The semi-logarithmic two-parameter LSS model (Eq. (6) shows less good prediction (approx. 7% deviation of the predicted retention times from the experiment) mainly for weakly retained phenolic acids (gallic, protocatechuic, ferulic, sinapic), rutin and 4-hydroxycoumarin, i.e. for weakly retained compounds. The Eq. (9) shows largest deviations from the experiment (> 10%), even though the gradient started at only 3% acetonitrile. Hence, the last model is the least suitable for prediction of retention in fast gradients starting at non-zero concentrations of organic solvents.

4.2.3. Effects of the Dwell Volume in Gradient Models

The instrumental gradient delay time, t_D, is considered in the Eqs. (6)–(9), to account for a shorter or a longer distance some less retained compounds may move along the column in the starting mobile phase before the front of the gradient. Some weakly retained compounds may even completely elute from the column in the dwell volume of the instrument under isocratic conditions ($V_R < V_D$). The gradient pre-elution is more likely to occur on columns with low hold-up volume (V_m) with respect to V_D. For example, benzene completely elutes from the short, 25 mm, Chromolith Flash RP-18e column, in the dwell volume before the on-set of the 1 min gradient 50–100% ACN (Table 3).

The implementation of the gradient dwell volume into the model equations for gradient elution is not only important for correct prediction of retention, but offers possibility for calculating the dwell volume from the model equations from the difference between the experimental elution volume of retained sample and its predicted elution volume calculated after deliberately setting $V_D = 0$. Table 3 illustrates this approach for the two Chromolith columns. The application of the gradient models described by Eqs. (6)–(8) yield V_D values (0.91–0.95 mL) in good agreement with the traditionally determined dwell volume measured in blank acetone gradient in acetonitrile with disconnected column (0.94 mL). This further confirms good validity of the theoretical gradient models to the gradients of acetonitrile in water on the Chromolith columns.

4.3. Gradient peak widths

Under constant isocratic conditions (column, temperature, mobile phase composition and flow rate), the height equivalent to the theoretical plate, H, and the number of theoretical plates, N, are approximately constant; hence the bandwidths increase for later eluting compounds (higher k_e). The isocratic numbers of theoretical plates, N, of alkylbenzenes calculated from the $H \approx 10$ μm at 5 mL/min in 60% acetonitrile, was $N = 5000$ for the 5 cm Chromolith HR RP-18e and 2100 for the 2.5 cm Chromolith Flash RP-18e – (Fig. 1).

Table 6 shows the experimental gradient peak widths, w_g, at the baseline (4σ, in minutes) for alkylbenzenes, in fast 1 min gradients, corrected for the extra-column contributions using Eq. (17). As expected, the peak widths are wider on the 2.5 cm, less efficient Chromolith Flash column than on the 5 cm Chromolith HR column, and for shorter gradients starting at 50% acetonitrile, in comparison with the full 0–100% ACN gradients. These results are consistent with our recent study of fast gradients on core–shell columns [4].

4.3.1. Retention Factors and Actual Mobile Phase Composition at the Time of Elution

The gradient retention models of Eqs. (6)–(9) can be easily adapted to calculate not only the retention factors, k_e, at the time of elution (Eqs. (12)–(15). Table 6 shows the predicted values of k_e of alkylbenzenes and the corresponding volume fractions of acetonitrile at the time of elution, φ_e, for the four gradient models. The log–log model (Eq. (13)) and the three-parameter models (Eqs. (14) and (15)) predict significantly higher k_e, for butylbenzene and pentylbenzene than the LSS model (Eq. (12)). In comparison with gradients starting at 0% acetonitrile, the concentration of acetonitrile at the time of elution, φ_e, are lower and k_e are higher for gradients starting at 50% acetonitrile.

4.3.2. Gradient Number of Theoretical Plates

The experimental gradient peak widths at 4σ, $w_{g(av)}$ were very similar for the individual sample compounds eluting during a gradient on the monolithic columns (0.0152 min in the gradient 0–100% ACN and 0.0234 min in the 1 min gradient 50–100% ACN for the Chromolith Flash column; 0.0146 min in the 1 min gradient 0–100% ACN and 0.0204 min in the 1 min gradient 50–100% ACN for the Chromolith HR column). Hence the mean $w_{g(av)}$ could be used to calculate the gradient number of theoretical plates, $N_{(g)}$, from Eq. (16), with the individual k_e at the time of elution predicted by the semi-logarithmic (Eq. (12)), log–log (Eq. (13)) and three-parameter (Eqs. (14) or (15)) models for 1 min 0–100% and 0–50% ACN gradients. The calculated gradient plate numbers, $N_{(g)}$ are given in Table 6.

The k_e and $N_{(g)}$ could not be determined for benzene, pre-eluting in the dwell volume in the 50–100% ACN gradients from the 25 mm long Flash column, where also the data for early eluted methylbenzene are not reliable. This applies also for benzene and methylbenzene on the Chromolith High Resolution column. For the rest of the compounds, the predicted $N_{(g)}$ depend not only on the type of column and on the gradient concentration range, but also on the gradient model employed, possibly due to slight differences in the predicted profile of changing retention during gradient elution. The log–log model (Eq. (13)) or the three-parameter model (Eq. (14)) provide closer values of k_e and lower differences in $N_{(g)}$ between the individual alkylbenzenes than the semi-logarithmic model (Eq. (12)), especially for the 0–100% ACN gradients.

4.4. Modeling gradient separation

We used the average experimental peak widths (Table 6) and the retention times predicted using four retention models (Table 4), for constructing chromatograms of alkylbenzenes in 1 min gradients (0–100 and 50–100% ACN). The predicted separations are compared with the experimental chromatograms in Fig. 3 for the Chromolith Flash and in Fig. 4 for the Chromolith High Resolution columns. All predicted chromatograms show relatively good

Table 5
Experimental, $t_{R,exp}$, and calculated, $t_{R,calc}$, elution times of phenolic acids and flavones on the Chromolith HighResolution column. $\Delta\ t_R$ are % differences in t_R. Gradient: 3–60% ACN in 2 min; flow rate 5 mL/min.

Compounds	$t_{R,exp}$ (min)	log k–φ (Eq. 6) $t_{R,calc}$ (min)	$\Delta\ t_R$ (%)	log k–log φ (Eq. 7) $t_{R,calc}$ (min)	$\Delta\ t_R$ (%)	k–φ (Eq. 8) $t_{R,calc}$ (min)	$\Delta\ t_R$ (%)	k–φ (Eq. 9) $t_{R,calc}$ (min)	$\Delta\ t_R$ (%)
Gallic acid	0.311	0.208	33.1	0.324	4.2	0.316	1.7	0.356	14.5
Protocatechuic a.	0.505	0.439	13.2	0.508	0.6	0.446	11.7	0.462	8.4
Esculin	0.630	0.576	8.5	0.592	6.0	0.576	8.6	0.572	9.2
PHBA	0.643	0.588	8.5	0.618	3.8	0.589	8.4	0.581	9.6
Vanillic acid	0.674	0.673	0.2	0.686	1.8	0.676	0.3	0.637	5.4
Chlorogenic acid	0.674	0.627	6.9	0.631	6.3	0.628	6.8	0.598	11.3
(+)-Catechin	0.689	0.710	3.1	0.621	9.9	0.658	4.5	0.576	16.4
4-HPAC	0.705	0.655	7.1	0.669	5.1	0.657	6.8	0.625	11.3
Caffeic acid	0.726	0.689	5.1	0.699	3.7	0.693	4.6	0.657	9.5
Syringic acid	0.761	0.704	7.5	0.717	5.8	0.714	6.2	0.657	13.7
(-)-Epicatechin	0.789	0.787	0.2	0.710	10.0	0.723	8.4	0.654	17.1
Coumaric acid	0.874	0.803	8.1	0.834	4.6	0.824	5.7	0.781	10.6
Rutin	0.910	0.814	10.5	0.876	3.8	0.859	5.6	–[a]	–
Ferulic acid	0.936	0.842	10.1	0.901	3.8	0.887	5.3	0.822	12.2
Sinapic acid	0.936	0.839	10.4	0.900	3.8	0.886	5.3	0.835	10.8
Salicylic acid	0.955	0.897	6.1	0.935	2.1	0.904	5.4	0.893	6.5
Hesperidin	1.047	1.025	2.1	1.029	1.7	1.030	1.6	0.942	10.1
Naringin	1.070	1.076	0.5	1.077	0.7	1.078	0.7	0.987	7.8
Myricetin	1.082	1.024	5.4	1.045	3.4	1.043	3.6	0.929	14.1
4-hydroxycoumarin	1.094	0.979	10.5	1.113	1.7	1.046	4.4	1.001	8.5
Quercetin	1.253	1.216	2.9	1.214	3.1	1.213	3.2	1.090	13.0
Naringenin	1.376	1.334	3.1	1.338	2.7	1.338	2.7	1.239	10.0
Apigenin	1.380	1.338	3.0	1.344	2.6	1.342	2.8	1.212	12.1
Hesperetin	1.427	1.378	3.4	1.390	2.6	1.387	2.8	1.260	11.7
7-Hydroxyflavon	1.458	1.395	4.3	1.415	3.0	1.400	4.0	1.304	10.6
Flavone	1.767	1.643	7.0	1.746	1.2	1.723	2.5	1.609	9.0
Biochanin A	1.780	1.649	7.4	1.758	1.3	1.731	2.8	1.624	8.8
Average differences (%)		7.0		3.2		4.5		10.7	

[a]Statistically not significant parameters of Eq. (4) for calculation t_R.

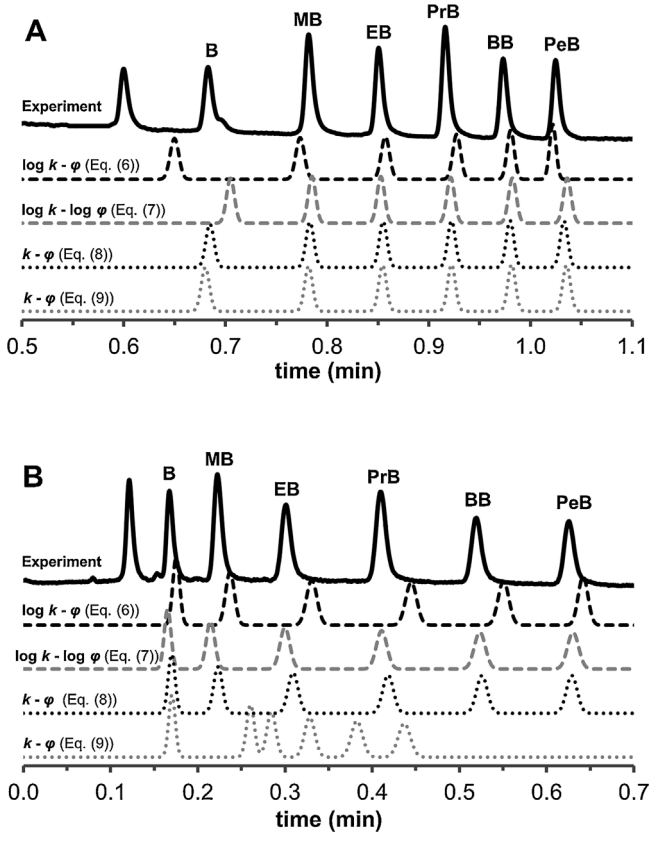

Fig. 3. Predicted chromatogram of alkylbenzenes using four retention models Eqs. (6)–(9) for gradient 0–100% ACN in 1 min (A) and for gradient 50–100% ACN in 1 min (B) on the Chromolith Flash column. Mobile phase: water + acetonitrile; flow rate: 5 mL/min; temperature: 40 °C.

Fig. 4. Predicted chromatograms of alkylbenzenes using four retention models Eqs. (6)–(9) for gradient 0–100% ACN in 1 min (A) and for gradient 50–100% ACN in 1 min (B) on the Chromolith High Resolution column. Mobile phase: water + acetonitrile; flow rate: 5 mL/min; temperature: 40 °C.

Table 6
Experimental (exp) values of the peak width, $w_{(g)}$, calculated gradient plate numbers, $N_{(g)}$, retention factors at the time of elution, k_e, and volume fractions at the time of elution, φ_e, for four retention models. Gradient 0–100% ACN in 1 min and 50–100% ACN in 1 min, flow rate 5 mL/min, gradient dwell time 0.19 min.

Gradient 0–100% acetonitrile in 1 min

		Chromolith Flash											
		log k–φ (Eq. 6)			log k–log φ (Eq. 7)			k–φ (Eq. 8)			k–φ (Eq. 9)		
Comp.	$w_{(g),exp}$ (min)	$N_{(g)}$	$k_{e,calc}$	$\varphi_{e,calc}$ (% 10^{-2})	$N_{(g)}$	$k_{e,calc}$	$\varphi_{e,calc}$ (% 10^{-2})	$N_{(g)}$	$k_{e,calc}$	$\varphi_{e,calc}$ (% 10^{-2})	$N_{(g)}$	$k_{e,calc}$	$\varphi_{e,calc}$ (% 10^{-2})
B	0.017	3795	1.86	0.38	3372	1.69	0.43	3595	1.78	0.41	3386	1.70	0.41
MB	0.016	3648	1.80	0.50	3102	1.58	0.51	3300	1.66	0.51	3198	1.62	0.51
EB	0.016	3477	1.73	0.59	3136	1.60	0.58	3218	1.63	0.58	3062	1.57	0.58
PrB	0.015	3115	1.59	0.66	3234	1.64	0.65	3138	1.60	0.65	2978	1.53	0.65
BB	0.014	2641	1.38	0.71	3329	1.68	0.71	3092	1.58	0.71	2966	1.53	0.71
PeB	0.015	2107	1.13	0.75	3344	1.68	0.77	3135	1.60	0.76	3068	1.57	0.77
		Chromolith HighResolution											
		log k–φ (Eq. 6)			log k–log φ (Eq. 7)			k–φ (Eq. 8)			k–(Eq. 9)		
Comp.	$w_{(g),exp}$ (min)	$N_{(g)}$	$k_{e,calc}$	$\varphi_{e,calc}$ (% 10^{-2})	$N_{(g)}$	$k_{e,calc}$	$\varphi_{e,calc}$ (% 10^{-2})	$N_{(g)}$	$k_{e,calc}$	$\varphi_{e,calc}$ (% 10^{-2})	$N_{(g)}$	$k_{e,calc}$	$\varphi_{e,calc}$ (% 10^{-2})
B	0.015	6992	1.00	0.50	7109	1.02	0.52	6733	0.96	0.51	6880	0.99	0.51
MB	0.015	6920	0.99	0.60	6348	0.91	0.60	6722	0.96	0.60	6609	0.95	0.60
EB	0.015	6714	0.96	0.67	6081	0.87	0.66	6590	0.94	0.66	6513	0.93	0.66
PrB	0.015	6351	0.91	0.74	6133	0.87	0.72	6514	0.93	0.73	6604	0.95	0.73
BB	0.014	5744	0.81	0.78	6370	0.91	0.78	6433	0.92	0.78	6754	0.97	0.79
PeB	0.014	5060	0.70	0.82	6773	0.97	0.83	5991	0.85	0.83	6928	0.99	0.84

Gradient 50–100% acetonitrile in 1 min

		Chromolith Flash											
		log k–φ (Eq. 6)			log k– log φ (Eq. 7)			k–φ (Eq. 8)			k–φ (Eq. 9)		
Comp.	$w_{(g),exp}$ (min)	$N_{(g)}$	$k_{e,calc}$	$\varphi_{e,calc}$ (% 10^{-2})	$N_{(g)}$	$k_{e,calc}$	$\varphi_{e,calc}$ (% 10^{-2})	$N_{(g)}$	$k_{e,calc}$	$\varphi_{e,calc}$ (% 10^{-2})	$N_{(g)}$	$k_{e,calc}$	$\varphi_{e,calc}$ (% 10^{-2})
B [a]	0.016	–	–	–	–	–	–	–	–	–	–	–	–
MB	0.020	2060	2.24	0.48	1710	1.95	0.47	1843	2.06	0.48	969	1.22	0.49
EB	0.023	2818	2.78	0.53	2285	2.41	0.51	2432	2.52	0.52	1295	1.57	0.51
PrB	0.025	3152	3.00	0.59	2686	2.69	0.57	2746	2.74	0.57	1680	1.92	0.53
BB	0.024	2972	2.89	0.64	2903	2.84	0.63	2824	2.79	0.63	2028	2.21	0.56
PeB	0.025	2417	2.50	0.69	2930	2.86	0.68	2809	2.78	0.68	2352	2.46	0.58
		Chromolith HighResolution											
		log k–φ (Eq. 6)			log k–log φ (Eq. 7)			k–φ (Eq. 8)			k–φ (Eq. 9)		
Comp.	$w_{(g),exp}$ (min)	$N_{(g)}$	$k_{e,calc}$	$\varphi_{e,calc}$ (% 10^{-2})	$N_{(g)}$	$k_{e,calc}$	$\varphi_{e,calc}$ (% 10^{-2})	$N_{(g)}$	$k_{e,calc}$	$\varphi_{e,calc}$ (% 10^{-2})	$N_{(g)}$	$k_{e,calc}$	$\varphi_{e,calc}$ (% 10^{-2})
B	0.019	4420	1.24	0.49	3748	1.06	0.48	4060	1.14	0.49	2695	0.75	0.51
MB	0.020	5768	1.55	0.55	4690	1.30	0.53	4982	1.37	0.53	3398	0.96	0.52
EB	0.021	6500	1.71	0.60	5272	1.44	0.58	5467	1.49	0.58	4059	1.14	0.54
PrB	0.021	6595	1.73	0.66	5677	1.53	0.63	5758	1.55	0.64	4797	1.33	0.56
BB	0.021	6003	1.60	0.71	5824	1.57	0.69	5822	1.57	0.69	5415	1.47	0.59
PeB	0.020	5081	1.40	0.75	5831	1.57	0.74	6198	1.65	0.75	5922	1.59	0.62

[a] Elution before gradient in 50% ACN.

agreement with the experiment in the full-range gradient (0–100% acetonitrile, A), only the two-parameter semi-logarithmic (LSS) model results in slightly lower predicted elution volume for the earliest eluted benzene. However, the three-parameter model of Eq. (9) provides unacceptably poor prediction for the gradients from 50 to 100% acetonitrile, as discussed earlier. The three-parameter model described by Eq. (8) provides the best agreement with the experiment for the two 1 min gradients on the two Chromolith columns.

In the optimization of gradient elution within a fixed gradient time range (such as 1 min), one should consider the effect of the starting gradient concentration, A, on the gradient bandwidths. The data in Table 6 show that the peak widths increase at higher starting gradient volume fractions of acetonitrile. The effect of the starting gradient concentration, A, on the gradient bandwidths of alkylbenzenes, $w_{(g)}$, could be estimated by extrapolation (linear to first approximation) from the experimental data for 0–100% and 50–100% ACN gradients (1 min). The peak widths for all alkylbenzenes eluting during a given gradient run are shown as the intervals for the two Chromolith columns in Fig. 5a. The 50 mm Chromolith HR column provides lower peak widths and narrower w_g intervals than the 25 mm Chromolith Flash column. However, there were only minor differences between the peak widths of the individual alkylbenzenes, so that average w_g could be considered in calculations of the gradient plate numbers, $N_{(g)}$.

In addition to the gradient bandwidths, the acetonitrile concentration at the start of the gradient, A, strongly affects the retention factors at the time of elution, k_e, as show Eqs. (12) (15), which predict decreasing k_e at increasing starting concentrations of ACN, A. At a constant gradient time, $t_G = \Delta t$, however, increasing A is automatically connected with decreasing gradient slopes, B:

$$B = \frac{\Delta\varphi}{t_G} = \frac{\varphi_G - A}{t_G} \quad (18)$$

The decreasing gradient ramp, B, counteracts the direct effect of the starting ACN concentration, A on k_e and consequently it causes less steep decrease of the gradient number of theoretical plates, $N_{(g)}$, in the interval between 0.05 and 0.35 on the Chromolith Flash column, an at 0.15–0.40, i.e. for gradients starting at 15–40% ACN on the Chromolith HR column, as shows Fig. 5b.

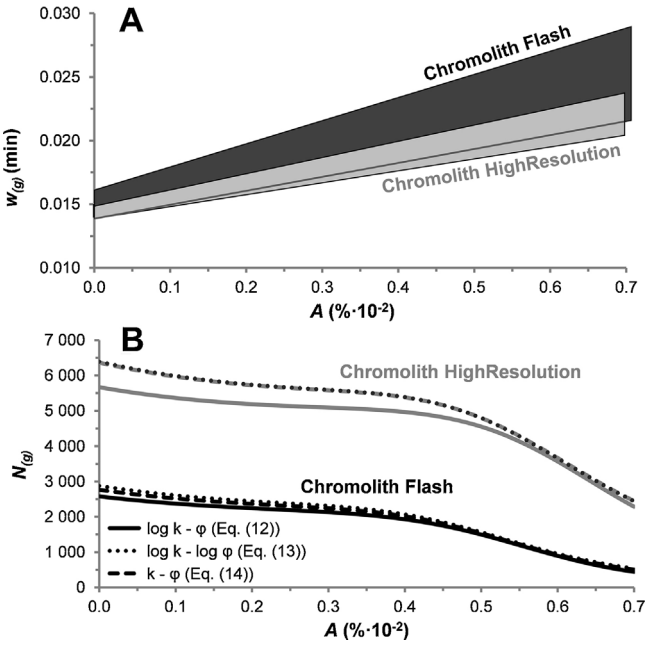

Fig. 5. (A) Estimated change in the gradient bandwidths of alkylbenzenes, $w_{(g)}$, at increasing volume fraction of acetonitrile at the start of 1 min gradient, *A*, based on the experimental data for 0–100% and 50–100% ACN gradients (1 min). (B) Effect of the ACN concentration at the start of a 1 min gradient, *A*, on the gradient number of theoretical plates, $N_{(g)}$, – Eq. (18). I: a 25 mm Chromolith Flash column, II: a 50 mm Chromolith HighResolution column.

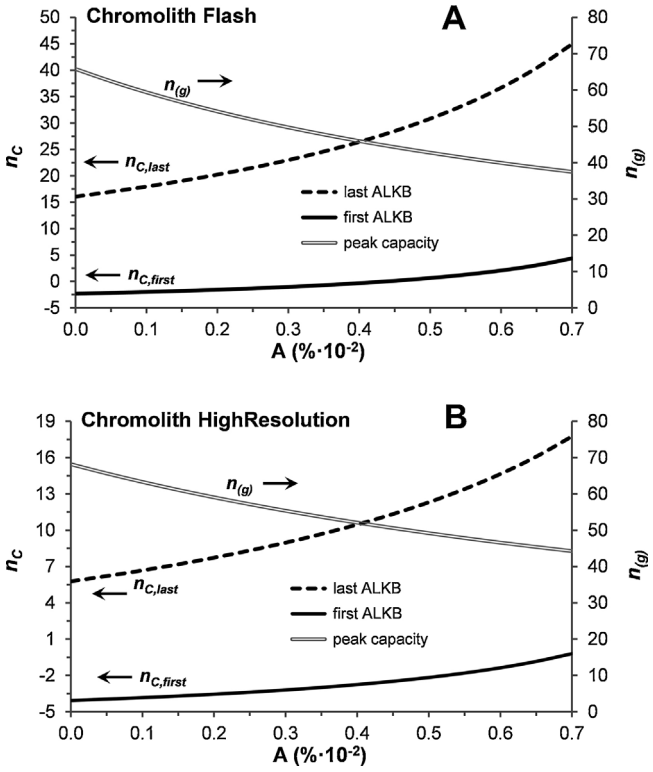

Fig. 6. Effect of the ACN concentration at the start of the gradient, *A*, on the theoretical gradient peak capacities, $n_{(g)}$, – Eq. (16). (A) a 25 mm Chromolith Flash column; (B) a 50 mm Chromolith HighResolution column. $n_{c,first}$, and $n_{c,last}$, are theoretical equivalents of the numbers of carbon atoms in the alkyl of the first and the last, respectively, alkylbenzenes eluted during the gradient time (1 min).

4.5. Peak capacity and 2D separations of phenolic acids and flavones

The gradient peak capacity, n_g, i.e. the number of peaks that can be accommodated within the gradient time range, Δt_R, defined by the first and the last peak eluted in the gradient, can be estimated from Eq. (9), assuming a constant gradient bandwidth, $w_{(g)}$, or using an average gradient number of theoretical plates, $N_{(g)}$, and the average retention factor at the time of elution, k_e, calculated from Eqs. (12)–(14) [13,40]:

$$n_{(g)} = \frac{\Delta t_R}{w_{(g)}} + 1 = \frac{\sqrt{N_{(g)}}}{4} \frac{\Delta t_R}{t_0 (1 + k_e)} + 1 \quad (19)$$

As calculating $N_{(g)}$, may be less accruable it is more practical assuming a constant average gradient peak width, $w_{(g)}$,[16] to estimate the theoretical (maximum) gradient peak capacity, $n_{(g)}$. If we are limited by a fixed short separation time, Δt_R, such as in the second dimension of comprehensive LC × LC, the peak capacity can be adjusted by setting the flow rate of the mobile phase and the gradient range, i.e. the mobile phase composition at the start (*A*) and at the end (φ_g) of the gradient. The optimum flow rate for fast separation is usually close to the maximum allowed by the experimental pressure limits. Hence, columns with high permeability and low flow resistance should be used, whenever possible, such as core–shell or monolithic columns [14]. At the optimum flow rate, appropriate adjustment of the gradient mobile phase composition range provides the most efficient optimization tool for gradient separations [8,11–13]. The gradient range may affect sample peak capacity equally or even more significantly than the length of monolithic columns or of columns packed with core–shell particles [28].

Fig. 6 shows the effect of the starting gradient concentration of ACN, *A*, on decreasing total gradient peak capacity, $n_{(g)}$, (right *Y*-axis) on the Chromolith Flash, 25 mm, column and on the Chromolith HR, 50 mm, column at the maximum mobile phase flow rate of 5 mL/min. The gradient peak capacity is higher for the more efficient 50 mm Chromolith HR column, with respect to the shorter 25 mm Chromolith Flash column, however, the difference is much lower than it could be expect from the ratio of the double column length, due to increased ratio $\Delta t_R/t_0$ on the latter column, which largely compensates for a higher number of theoretical plates of the Chromolith HR column (Table 2). The figure shows also the theoretical equivalents of the numbers of carbon atoms in the alkyls of the first ($n_{c\ first}$, full line) and the last ($n_{c,last}$, dashed line) ABs, respectively, alkylbenzenes eluted in the gradient time interval (1 min) (left *Y*-axis). The numbers characterize the lipophility interval of the compounds likely to elute during 1 min gradients, which significantly increases at the gradients shifting to higher start concentrations of acetonitrile. Hence, by adjusting the gradient range, it is possible to fit the gradient to the expected lipophilicity of samples [10]. At lower starting concentrations of ACN, the lipophilicity interval is significantly broader for the Chromolith Flash column.

Table 7 shows the peak capacities, $n_{(g)calc}$, calculated from Eq. (19) for different models and the average gradient bandwidths of Table 6. The calculated theoretical peak capacities are compared with the experimental values, $n_{(g)}$, determined by dividing the gradient time (1 min) + the gradient dwell time (0.19 min, equal to the gradient re-equilibration time) by the average experimental gradient peak width. The log–log (Eq. (7)) and the three-parameter (Eq. (8)) gradient models provide very similar predicted peak capacities, ca. 2–4% lower than the experimental $n_{(g)}$. The semi-logarithmic model (Eq. (6) provides slightly worse prediction agreement. Because the peak capacities are directly proportional to the square root of the gradient plate number, they are higher for the gradients from 0 to 100% ACN, which yield more compressed peaks than the gradients from 50 to 100% ACN.

Table 7
Theoretical gradient peak capacity, $n_{(g)}$, for alkylbenzenes (calculated for propylbenzene) and for phenolic acids and flavones (calculated from average $w_{(g)}$) and average peak width $w_{(g)}$, average gradient number of theoretical plate, $N_{(g)}$, correlated gradient peak capacity, $n'_{(g)}$, between benzene (as first peak) and last eluted peak eluted at the time of the end gradient. $n_{c,last}$, theoretical equivalents of the numbers of carbon atoms in the alkyls of the last alkylbenzene in the gradient time interval, N.B., number of bins in 2D separation space (ideal two-dimensional peak capacity, ($n_{2D} = n_{D1} \times n_{D2}$); *C.S.S.*, coverage of two-dimensional separation space; R^2, correlation coefficient; s^2, selectivity coefficient ($s^2 = 1 - R^2$).

Column	Gradient range (% ACN)	Gradient time (min)	F_m (min)	$w_{(g)}$ (min)	$n_{(g)}$	$n_{(g),calc}$ (Eq. (1))	$n_{(g),calc}$ (Eq. (2))	$n_{(g),calc}$ (Eq. (3))	$N_{(g)}$	$n'_{(g)}$	$n_{c,last}$
alkylbenzenes											
Chromolith Flash	0–100	1.0	5	0.015	80	75	78	79	3200	34	16
	50–100	1.0	5	0.024	49	48	49	48	2500	42	31
Chromolith HighResolution	0–100	1.0	5	0.015	86	79	83	81	6500	23	6
	50–100	1.0	5	0.021	58	53	57	57	5 500	42	12
phenolic acids and flavones						N.B.	*C.S.S.* (%)	R^2	s^2		
1D separation											
Chromolith Flash	3–40	2.0	5	0.024	85	–	–	–	–		
Chromolith HighResolution	3–60	2.0	5	0.019	105	–	–	–	–		
2D separation (Fig. 7)											
D1: BiGDMA-MEDSA	95–70	70.0	0.004	3.289	21	756	9.9	0.272	0.728		
D2: Chromolith Flash	1–55	0.8	5	0.022	36						
D1: BiGDMA-MEDSA	95–70	70.0	0.004	3.489	20	900	8.5	0.239	0.761		
D2: Chromolith HighResolution	5–60	1.0	5	0.022	45						

However, the gradient peak capacity, $n'_{(g)}$, actually available for separation of alkylbenzenes between the elution time of the relatively weakly retained benzene and the end time of the gradient at 100% acetonitrile (1 min). $n'_{(g)} = n_{c,last}$ gives a more realistic picture of the lipophilicity sample range, which is higher in gradients starting at 50% ACN, in comparison with the "full" gradients (0–100% ACN). Due to higher peak capacity, the longer Chromolith High Resolution column allows separating a higher number of compounds, but within a lower lipophilicity range than shorter Chromolith Flash column in the same gradient time. This increase could be even more significant for gradients ending at less than 100% acetonitrile. Gradients starting at a non-zero concentration of acetonitrile provide more efficient use of the earlier parts of the chromatograms and obviously would enable separation of some higher alkylbenzenes $n_{c,last}$ (Table 7).

Table 7 further shows the peak capacities for the gradients optimized for the separations of phenolic acids and (or) flavones for 2 and 0.8 min or 1 min gradients. The peak capacities are higher on the more efficient 5 cm Chromolith HighResolution column, but the 2.5 cm short Chromolith Flash column shows also interestingly high peak capacities, which strongly depend on the gradient range.

Fig. 7 shows two-dimensional comprehensive "monolithic" LC × LC separations of 30 phenolic acids and flavones, using a 0.53 mm, i.d. monolithic polymethacrylate zwitterionic HILIC microcolumn in the first dimension, combined with either the Chromolith Flash RP 18-E or the Chromolith HighResolution RP 18-E columns in the second dimension. The first-dimension peak width on the BiGDMA-MEDSA microcolumn is in agreement with the Murphy–Schure–Foley criterion [47], requiring that the effluent from the first dimension should be sampled at least three to four

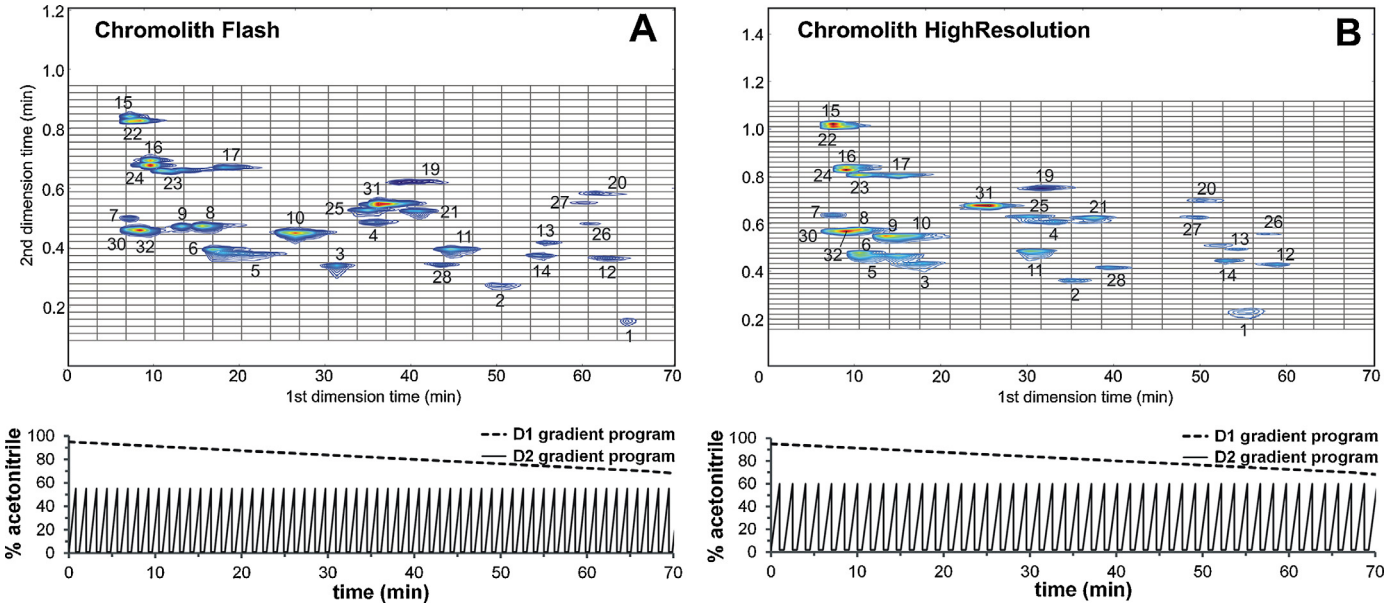

Fig. 7. 2D separations of phenolic acids and flavones. Comprehensive LC × LC separation of phenolic acids and flavones on a zwitterionic polymethacrylate 210 mm × 0.53 mm i.d. monolithic column (60 °C) in the first dimension and a Chromolith HighResolution 50 mm × 4.6 mm i.d. column (A) or a Chromolith Flash 25 mm × 4.6 mm i.d. column (B) (50 °C) in the second dimension, using simultaneous gradient elution in the HILIC × RP setup. The mobile phase consisted of 0.01 mol/L ammonium acetate in water (pH 3.1) plus 0.01 mol/L ammonium acetate in acetonitrile. The profiles of the acetonitrile gradients are shown as dashed lines in the first dimension D1 and as full lines in the second dimension (D2 – repeated gradients from 0 to 60% ACN in 1 min for the analysis of repeated collected fractions). The interface consisted of 10-μL sampling loops, with a switching time of 1.5 min.

times over the width of a first dimension peak to avoid significant loss of 2D resolution due to undersampling. The first-dimension monolithic column can be operated also in the RP mode (an RP × RP setup) [46]. The details of the two-dimensional setup including the home-made monolithic zwiterionic polymethacrylate 0.53 mm, i.d. BiGDMA–MEDSA HILIC micro-column in the first dimension were as published earlier [46]. The orthogonality coefficients $s^2 = 1-R^2$, characterizing the differences in the separation selectivities of the two dimensions, are complementary to the correlation coefficient, R^2, between the retention times in the two coupled separation systems. The HILIC × RP setups with the Chromolith Flash and the Chromolith HR columns in the second dimension, offer higher s^2 coefficients (0.728 or 0.761, respectively; Table 7), than the HILIC × RP setups using the same BiGDMA–MEDSA micro-column in the first dimension and a core–shell column Kinetex XB-C18 in the second dimension (not shown, $s^2 = 0.69$, [46]). Fig. 7a shows the HILIC × RP setup with the monolithic polymethacrylate zwitterionic microcolumn in the first dimension and the Chromolith Flash RP-18E in the second dimension. Here, the two-dimensional peak capacity is slightly lower, however, the difference from the setup including the longer and more efficient Chromolith HR column (Fig. 7b) is low enough to still allow efficient using the short 2.5 cm Chromolith Flash column in 2D applications. The useful two-dimensional separation space and corresponding peak capacities are illustrated as a grid in two-dimensional comprehensive separations in Fig. 7. The Chromolith HR column in the second dimension provided a higher two-dimensional peak capacity, but lower coverage of the two-dimensional separation space (C.S.S. = 8.5%) than Chromolith Flash column (C.S.S. = 9.9%). All phenolic acids and flavones were almost completely separated in 70 min in contrast to one-dimensional separations in Fig. 2, where 4 from 27 compounds on the Chromolith Flash column and 7 from 32 compounds on the Chromolith HR column were overlapping.

5. Conclusions

1. We tested four models direct calculations of the gradient elution data for prediction retention in fast (1 min) gradients of acetonitrile in water on two C18 silica monolithic columns. The second-generation Chromolith HighResolution 50 mm column provided improved separation efficiency with respect to the first-generation Chromolith Flash 25 mm column. The prediction errors of all gradient models tested were in between 0.7 and 1.5% of retention times of alkylbenzenes, phenolic acids and flavones for fast 1 min gradients starting in pure water, which proves that the validity of the models is not affected by the monolithic character of the separation medium in short columns and that the equilibration in the column during the gradient elution is fast enough not to cause distortion of the gradient profile even as flow rates as fast as 5 mL/min. For 1 min gradients starting at higher concentrations of acetonitrile, the log–log two-parameter retention model and a simple (1978) three-parameter retention model provided prediction errors in between 1.16 and 4.5%, whereas the traditionally used semi-logarithm two-parameter model traditionally used in reversed-phase chromatography yielded prediction errors in between 3.7 and 7.4%, probably because some positive deviations from linearity in low ACN concentration range. The recent (2010) three-parameter model was connected with larger prediction errors, up to 20%.

2. The individual gradient retention models show some differences in the k_e values used for calculations of the theoretical plates in gradient elution, $N_{(g)}$, based on the average experimental peak widths for the sample compounds eluting during the gradient. This approach allowed gradient modeling in fast 1 min gradients with the errors in prediction close to range of the errors of the repeated experimental measurements.

3. For short gradients run at high flow rates close to the instrumental limits within a fixed gradient time (1 min or less), appropriate selection of the gradient range (the concentrations of the strong solvent B at the start and at the end of the gradient) is more important for optimum resolution and peak capacities, than the length of the column used. The monolithic columns show very flat $H–u$ plots and high permeability, so that they can be operated at a high flow rate of the mobile phase, up to 5 mL/min, without significant sacrifice in separation efficiency (H). This enables relatively high volumes (up to 5 mL) of the mobile phase to be used within the short gradient time of 1 min and increasing the peak capacity of 2D separations with respect to columns packed with fully porous particles.

4. The peak capacities of the two short Chromolith columns were high enough to allow their efficient use for fast gradient chromatography in the second (reversed-phase) dimension of comprehensive 2D HPLC, in combination with a polar monolithic microcolumn in the first dimension, which can be operated either in HILIC or in RP mode.

Appendix A. Supplementary data

Supplementary data associated with this article can be found, in the online version, at http://dx.doi.org/10.1016/j.chroma.2015.07.070

References

[1] L.W. Potts, D.R. Stoll, X. Li, P.W. Carr, The impact of sampling time on peak capacity and analysis speed in on-line comprehensive two-dimensional liquid chromatography, J. Chromatogr. A 1217 (2010) 5700–5709.
[2] K. Vyňuchalová, P. Jandera, Possibilities of retention prediction in fast gradient liquid chromatography. Part 1: comparison of separation on packed fully porous, nonporous and monolithic columns, J. Chromatogr. A 1278 (2013) 37–45.
[3] J.J. DeStefano, S.A. Schuster, J.M. Lawhorn, J.J. Kirkland, Performance characteristics of new superficially porous particles, J. Chromatogr. A 1258 (2012) 76–83.
[4] P. Jandera, T. Hájek, K. Vyňuchalová, Retention and bandwidths prediction in fast gradient liquid chromatography. Part 2–Core–shell columns, J. Chromatogr. A 1337 (2014) 57–66.
[5] H. Minakuchi, K. Nakanishi, N. Soga, N. Ishizuka, N. Tanaka, Octadecylsilylated porous silica rods as separation media for reversed-phase liquid chromatography, Anal. Chem. 68 (1996) 3498–3501.
[6] P. Aggarwal, H.D. Tolley, M.L. Lee, Monolithic bed structure for capillary liquid chromatography, J. Chromatogr. A 1219 (2012) 1–14.
[7] D. Cabooter, K. Broeckhoven, R. Sterken, A. Vanmessen, I. Vandendael, K. Nakanishi, S. Deridder, G. Desmet, Detailed characterization of the kinetic performance of first and second generation silica monolithic columns for reversed-phase chromatography separations, J. Chromatogr. A 1325 (2014) 72–82.
[8] K. Hormann, T. Muellner, S. Bruns, A. Hoeltzel, U. Tallarek, Morphology and separation efficiency of a new generation of analytical silica monoliths, J. Chromatogr. A 1222 (2012) 46–58.
[9] F. Gritti, N. Tanaka, G. Guiochon, Comparison of the fast gradient performance of new prototype silica monolithic columns and columns packed with fully porous and core-shell particles, J. Chromatogr. A 1236 (2012) 28–41.
[10] P. Česla, T. Hájek, P. Jandera, Optimization of two-dimensional gradient liquid chromatography separations, J. Chromatogr. A 1216 (2009) 3443–3457.
[11] T. Hájek, P. Jandera, Columns and optimum gradient conditions for fast second-dimension separations in comprehensive two-dimensional liquid chromatography, J. Sep. Sci. 35 (2012) 1712–1722.
[12] P. Jandera, T. Hájek, P. Česla, Effects of the gradient profile, sample volume and solvent on the separation in very fast gradients, with special attention to the second-dimension gradient in comprehensive two-dimensional liquid chromatography, J. Chromatogr. A 1218 (2011) 1995–2006.
[13] P. Jandera, Programmed elution in comprehensive two-dimensional liquid chromatography, J. Chromatogr. A 1255 (2012) 112–129.
[14] B.J. VanMiddlesworth, J.G. Dorsey, Re-equilibration time of superficially porous silica based columns in gradient elution reversed phase liquid chromatography, J. Chromatogr. A 1218 (2011) 7158–7165.
[15] A. Beyaz, W. Fan, P.W. Carr, A.P. Schellinger, Instrument parameters controlling retention precision in gradient elution reversed-phase liquid chromatography, J. Chromatogr. A 1371 (2014) 90–105.
[16] L.R. Snyder, J.W. Dolan, High-Performance Gradient Elution. The Practical Application of the Linear-Solvent-Strength Model, Wiley, Hoboken, N.J., 2007.

[17] P. Jandera, J. Churáček, Gradient elution in liquid chromatography: I. The influence of the composition of the mobile phase on the capacity ratio (retention volume, band width, and resolution) in isocratic elution—theoretical considerations, J. Chromatogr. 91 (1974) 207–221.
[18] L.R. Snyder, J.W. Dolan, J.R. Gant, Gradient elution in high-performance liquid-chromatography. 1. Theoretical basis for reversed-phase systems, J. Chromatogr. 165 (1979) 3–30.
[19] L.R. Snyder, Role of the solvent in liquid–solid chromatography, Rev. Anal. Chem. 46 (1974) 1384–1393.
[20] P.J. Schoenmakers, H.A.H. Billiet, R. Tijssen, L. Degalan, Gradient selection in reverse-phase liquid-chromatography, J. Chromatogr. 149 (1978) 519–537.
[21] P. Jandera, M. Janderova, J. Churacek, Gradient elution in liquid-chromatography.8. Selection of optimal composition of mobile phase in liquid-chromatography under isocratic conditions, J. Chromatogr. 148 (1978) 79–97.
[22] M. Jaroniec, Partition and displacement models in reversed-phase liquid chromatography with mixed eluents, J. Chromatogr. A 656 (1993) 37–50.
[23] P.C. Lu, X.M. Lu, Development of a high-performance liquid chromatograph with artificial-intelligence, J. Chromatogr. 292 (1984) 169–188.
[24] M. McCann, J.H. Purnell, C.A. Wellington, Mixed-solvent theory for liquid chromatography, Faraday Soc. Symp. Ser. 15 (1980) 83–91.
[25] P. Nikitas, A. Pappa-Louisi, P. Agrafiotou, Effect of the organic modifier concentration on the retention in reversed-phase liquid chromatography: II. Tests using various simplified models, J. Chromatogr. A 946 (2002) 33–45.
[26] M.C. García-Álvarez-Coque, J.R. Torres-Lapasió, J.J. Baeza-Baeza, Models and objective functions for the optimisation of selectivity in reversed-phase liquid chromatography, Anal. Chim. Acta 579 (2006) 125–145.
[27] P. Jandera, Can the theory of gradient liquid chromatography be useful in solving practical problems? J. Chromatogr. A 1126 (2006) 195–218.
[28] P. Nikitas, A. Pappa-Louisi, Retention models for isocratic and gradient elution in reversed-phase liquid chromatography, J. Chromatogr. A 1216 (2009) 1737–1755.
[29] U.D. Neue, H.-J. Kuss, Improved reversed-phase gradient retention modeling, J. Chromatogr. A 1217 (2010) 3794–3803.
[30] J.J. Baeza-Baeza, C. Ortiz-Bolsico, J.R. Torres-Lapasió, M.C. García-Álvarez-Coque, Approaches to model the retention and peak profile in linear gradient reversed-phase liquid chromatography, J. Chromatogr. A 1284 (2013) 28–35.
[31] P. Jandera, Gradient elution in liquid column chromatography - Prediction of retention and optimization of separation, in: P.R. Brown, E. Grushka, S. Lunte (Eds.), Adv. Chromatogr. 43 (2005) 1-108.
[32] P. Jandera, J. Churáček, Gradient elution in liquid-chromatography.2. Retention characteristics (Retention volume, band width, resolution, plate number) in solvent-programmed chromatography—theoretical considerations, J. Chromatogr. 91 (1974) 223–235.
[33] P. Jandera, J. Churáček, Gradient Elution in Column Liquid Chromatography, Elsevier, Amsterdam, 1985.
[34] P. Jandera, J. Churáček, L. Svoboda, Gradient elution in liquid chromatography: X. Retention characteristics in reversed-phase gradient elution chromatography, J. Chromatogr. 174 (1979) 35–50.
[35] M.A. Quarry, R.L. Grob, L.R. Snyder, Measurement and use of retention data from high-performance gradient elution: Contributions from "non-ideal" gradient equipment, J. Chromatogr. 285 (1984) 1–18.
[36] P. Jandera, J. Churáček, Liquid chromatography with programmed composition of the mobile phase, Adv. Chromatogr. 19 (1980) 125–160.
[37] P. Jandera, M. Kučerová, Prediction of retention in gradient-elution normal-phase high-performance liquid chromatography with binary solvent gradients, J. Chromatogr. A 759 (1997) 13–25.
[38] P. Jandera, Gradient elution in normal-phase high-performance liquid chromatographic systems, J. Chromatogr. A 965 (2002) 239–261.
[39] F. Gritti, G. Guiochon, Band broadening in fast gradient high-performance liquid chromatography: application to the second generation of 4.6 mm I.D. silica monolithic columns, J. Chromatogr. A 1238 (2012) 77–90.
[40] U.D. Neue, Theory of peak capacity in gradient elution, J. Chromatogr. A 1079 (2005) 153–161.
[41] L.R. Snyder, J.W. Dolan, The linear-solvent-strength model of gradient elution, Adv. Chromatogr. 38 (1998) 115–187.
[42] L.R. Snyder, D.L. Saunders, Optimized solvent programming for separations of complex samples by liquid-solid adsorption chromatography in column, J. Chromatogr. Sci. 7 (1969) 195–208.
[43] H. Poppe, J. Paanakker, M. Bronckhorst, Peak width in solvent-programmed chromatography: I. General description of peak broadening in solvent-programmed elution, J. Chromatogr. 204 (1981) 77–84.
[44] F. Gritti, G. Guiochon, Performance of columns packed with the new shell Kinetex-C18 particles in gradient elution chromatography, J. Chromatogr. A 1217 (2010) 1604–1615.
[45] U.D. Neue, D.H. Marchand, L.R. Snyder, Peak compression in reversed-phase gradient elution, J. Chromatogr. A 1111 (2006) 32–39.
[46] P. Jandera, M. Staňková, T. Hájek, New zwitterionic polymethacrylate monolithic columns for one- and two-dimensional microliquid chromatography, J. Sep. Sci. 36 (2013) 2430–2440.
[47] R.E. Murphy, M.R. Schure, J.P. Foley, Effect of sampling rate on resolution in comprehensive two-dimensional liquid chromatography, Anal. Chem. 70 (1998) 1585–1594.